Atmos. Chem. Phys. Discuss., doi:10.5194/acp-2016-147, 2016
Manuscript under review for journal Atmos. Chem. Phys.
Published: 25 February 2016

Atmospheric Chemistry and Physics Discussions

Effects of atmospheric dynamics and aerosols on the thermodynamic phase of cold clouds

Jiming Li[1], Qiaoyi Lv[1], Min Zhang[1], Tianhe Wang[1],
Kazuaki Kawamoto[2] and Siyu Chen[1]

[1]Key Laboratory for Semi-Arid Climate Change of the Ministry of Education, College of Atmospheric Sciences, Lanzhou University, Lanzhou, China

[2]Graduate School of Fisheries Science and Environmental Studies, Nagasaki University, Nagasaki, Japan

Running Head: Effects of dynamics and aerosols on the cold cloud phase

Corresponding author: Jiming Li, Key Laboratory for Semi-Arid Climate Change of the Ministry of Education, College of Atmospheric Sciences, Lanzhou University, Lanzhou, Gansu 730000, China. (lijiming@lzu.edu.cn)

Atmos. Chem. Phys. Discuss., doi:10.5194/acp-2016-147, 2016
Manuscript under review for journal Atmos. Chem. Phys.
Published: 25 February 2016

Abstract

Based on the 4 years (2007–2010) of data from the CloudSat 2B-CLDCLASS-LIDAR product, the European Centre for Medium-Range Weather Forecasts Auxiliary (ECMWF-AUX) product and Cloud-Aerosol Lidar and Infrared Pathfinder Satellite Observation (CALIPSO) level 2 5km aerosol layer product, this study investigates the impact of atmospheric dynamics and aerosol on cold cloud (cloud top temperature< 0ºC) phase on a global scale in order to better understand the conditions under which supercooled liquid water will gradually transform to ice phase.

Our results show that the thresholds of parameter T_{ice} (is the temperature below which all clouds are ice), T_w (is the temperature above which all clouds are liquid) and n (is a shape parameter that controls the relationship between supercooled liquid cloud fraction (SCF) and cloud top temperature) aren't unique for the entire globe as many models adopted. The value of T_w ranges from -2ºC to -6ºC at the most regions of the globe, and decreases from high latitudes to tropics. For T_{ice}, its value is warmer (>-26ºC) in the typical stratocumulus regions than the values at the other regions (<30ºC). The geographic distributions of parameter n are closely linked to aerosol loading and meteorological parameters, and its value varies strongly from 0 to 5. By comparing the absolute and relative differences between different cloud phase schemes and observation, we suggest that the cloud phase scheme used in Community Atmosphere Model (version 3, CAM3) and CAM5 can be considered as a preferred option in the models, and the application of dynamic thresholds of T_{ice}, T_w and n will further improve the predictions of SCF, particularly over the region of poleward of 40°.

Statistical results indicate that aerosol effect on nucleation can't fully explain the all changes of cold cloud phase in our study. SCF at a given temperature also appears to be related to the different collocations of surface temperature, vertical velocity and lower-tropospheric static stability (LTSS). We find that strong vertical motion can also enhance glaciation process and reduce the SCF (or increase n value) as ice nuclei

Atmos. Chem. Phys. Discuss., doi:10.5194/acp-2016-147, 2016
Manuscript under review for journal Atmos. Chem. Phys.
Published: 25 February 2016

aerosol did, and force the supercooled water to glaciate at a warmer temperature. For same vertical motion, however, high LTSS (or low surface temperature) tends to increase the SCF and force the supercooled water to glaciate at a colder temperature. Unstable atmosphere (low LTSS and high surface temperature) in those strong ascent regions favors deep convective cloud, and further exhausts the supercooled water by strong precipitation rate. Our results verify the importance and regional of dynamical factors on the changes of cold cloud phase, have potential implications for further improving the parameterization of the cloud phase and determining the climate feedbacks.

Atmos. Chem. Phys. Discuss., doi:10.5194/acp-2016-147, 2016
Manuscript under review for journal Atmos. Chem. Phys.
Published: 25 February 2016

1. Introduction

Clouds play an important role in regulating the Earth's radiation budget and global hydrological cycle (Stephens, 2005). However, because observations are lacking and understanding of the physical processes involved in cloud formation is insufficient, clouds are also regarded as the greatest uncertainties in climate change predictions made by various climate models (Williams et al., 2003; Zhang et al., 2005; Klein et al., 2013). One of the primary challenges in better understanding the role of clouds in climate forcings and feedbacks involves determining how to more accurately define the cold cloud phase (cloud top temperature<0ºC) composition between 0ºC and -40ºC, with unsophisticated cloud phase schemes in GCMs (general circulation models; Li and Le Treut, 1992; Morrison et al., 2003; Tao, 2003; Tsushima et al., 2006). Currently, many models specify the fraction of liquid-phase clouds solely as a function of temperature (Doutriaux-Boucher and Quaas, 2004; Storelvmo et al., 2008; Song et al., 2012), related ice heterogeneous nucleation processes are not considered in some models because of the poor understanding of aerosol particles' ice nucleation ability, coating conditions and nucleation modes (e.g., deposition, immersion freezing, contact or condensation freezing) (Lohmann and Feichter, 2005). In view of the entirely different radiative and microphysical properties of ice and liquid particles, changes in the liquid-ice phase transition will significantly affect the Earth's radiation budget and precipitation efficiency (Fu et al., 1999; Fu, 2007; Sassen and Khvorostyanov, 2007; Sun et al., 2004, 2015). Thus, the oversimplification of cloud phases in climate models inevitably leads to large biases in the study of various climate feedbacks and the sensitivity of these models.

The Clausius-Clapeyron theory and laboratory results have indicated that liquid water particles can exist at a temperature threshold as low as -38ºC to -40ºC before homogeneous nucleation occurs (Roger and Yau, 1989). Studies based on Lidar data and satellite observations have further verified the existence of liquid water at temperatures as low as -30ºC to -40ºC (e.g., Intrieri et al., 2002; Naud et al., 2006; Shupe et al., 2006; Morrison et al., 2011). For example, using un-polarized, ground-based Lidar data from Chilbolton in Southern England, Hogan et al. (2003)

have found that 27% of clouds between -5ºC and -10ºC in Chilbolton contain a supercooled liquid-water layer, and this percentage falls steadily with temperature and reaches approximately zero at temperatures below -35ºC. Giraud et al. (2001) have used the Along-Track Scanning Radiometer (ATSR)-2 infrared data from the ERS-2 satellite to analyze the relationship between cloud phase and cloud top temperature. Their results have indicated that the probability of ice phase clouds decreases quasi-linearly with cloud top temperature from nearly 100% at around -33ºC to close to 0% at -10ºC. By using polarimetric satellite data, Doutriaux-Boucher and Quaas (2004) have also derived a global lower limit of -32°C for 100% of ice phase clouds. However, the lowest temperature thresholds at which liquid water particles can exist within various climate models vary dramatically from -15ºC (Smith,1990; Doutriaux-Boucher and Quaas, 2004) to -23ºC (Weidle and Wernli, 2008) to -40ºC (Del Genio et al., 1996; Collins et al., 2004). In addition, the relationship between the supercooled liquid cloud fraction (SCF) and cloud top temperature (CTT) in some models and reanalysis datasets is fixed with an exponent of 1.7 (Doutriaux-Boucher and Quaas, 2004) or 2 (Smith, 1990; Weidle and Wernli, 2008). The unique temperature thesholds and relations for the entire globe, regardless of their geographic or temporal variations, eventually lead to the SCF at a given cloud top temperature express considerable differences among GCMs. For example, the liquid water cloud fraction at -15ºC varies from 12% to 83% in six single column models (SCMs) used in a model comparison study of Arctic mixed-phase clouds (Klein et al., 2009; Morrison et al., 2009). The geographic and temporal variations of SCF at a given temperature are further complicated by several factors, including ice nuclei (IN) concentrations and dynamic conditions such as vertical motion (Naud et al., 2006; Choi et al., 2010; Zhang et al., 2015). Combined satellite observations and reanalysis datasets have the potential to yield global cloud phase statistics and to clarify the relationship between cloud phase and microphysical/dynamic processes. This information would aid in the design and evaluation of more physically based cloud phase partitioning schemes, improve calculations of clouds' radiative effects, and reduce uncertainties in cloud feedbacks within GCMs.

Atmos. Chem. Phys. Discuss., doi:10.5194/acp-2016-147, 2016
Manuscript under review for journal Atmos. Chem. Phys.
Published: 25 February 2016

The millimeter-wavelength cloud-profiling radar (CPR) on CloudSat (Stephens et al., 2002) and the cloud-aerosol Lidar with orthogonal polarization (CALIOP) (Winker et al., 2007) on CALIPSO (launched in late April 2006) can provide more accurate data related to the vertical structure of clouds, along with cloud phase information on a global scale (Hu et al., 2010; Li et al., 2010, 2015). The depolarization ratio and layer-integrated backscatter intensity measurements from CALIOP can help distinguish cloud phases (Hu et al., 2007, 2009). Using combined CALIOP/IIR/MODIS measurements, Hu et al. (2010) have compiled global statistics on the occurrence, liquid water content and fraction of supercooled liquid clouds; and they have further developed a new cloud thermodynamic phase parameterization. Cheng et al. (2012) have examined the effect of this new cloud phase parameterization within a climate simulation by replacing the default parameterization in the CAM4 with this new one. In addition, Choi et al. (2010) and Tan et al. (2014) have utilized the vertically resolved observations of clouds and aerosols from CALIPSO to analyze cold cloud phase changes and possible aerosol impacts at given temperatures. However, systematic studies of the statistical relationship between cloud phase and IN aerosol properties under different dynamic conditions on a global scale have received far less attention. In this study, we combine cloud phase information from CloudSat and CALIPSO, aerosol data from CALIPSO, and dynamic parameters from the ECMWF-AUX and ERA-interim reanalysis datasets to investigate the geographic and seasonal variations of different parameters' thresholds used in the cloud phase partitioning schemes of climate models. We also perform a preliminary evaluation of how well different cloud phase partitioning schemes can characterize the variation of the SCF at cloud top temperatures from -40ºC to 0ºC; and we further evaluate and discuss the effects of atmospheric dynamics and aerosols on cloud phase at a given temperature.

This paper is organized as follows: a brief introduction of all datasets used in this study is given in Section 2. Section 3 outlines the global distributions of several important cloud phase parameters used in the models, evaluates the performance of different cloud phase partitioning schemes and discusses the effects of atmospheric

Atmos. Chem. Phys. Discuss., doi:10.5194/acp-2016-147, 2016
Manuscript under review for journal Atmos. Chem. Phys.
Published: 25 February 2016

dynamics and aerosols on a cloud's thermodynamic phase. Important conclusions and discussion are presented in Section 4.

2. Datasets and methods

In the following study, 4 years (2007–2010) of data from the latest release of the CloudSat 2B-CLDCLASS-LIDAR (version 1.0) product (e.g., radar–LiDAR cloud classification), the ECMWF-AUX product and the CALIPSO level 2, 5 km aerosol layer product are collected to analyze the effects of atmospheric dynamics and aerosols on the thermodynamic phase of cold clouds on a global scale. To analyze the regional variability of the studied parameters, we divide the globe into $2^{\circ}\times6^{\circ}$ grid boxes and collect a valid sample set from each grid box. Only those results and findings derived from daytime data are provided in this study in order to support the analysis of the radiative effects of different cloud phases in parallel studies.

2.1 Meteorological reanalysis dataset

In this study, the temperature profiles and surface temperatures (that is, skin temperature) used in our analysis are taken from the ECMWF-AUX product (Partain, 2004), which is an intermediate product that contains the set of ancillary ECMWF state variable data interpolated to each CloudSat cloud profiling radar (CPR) bin. In addition to this information, the collocated vertical velocity parameter from the ERA-Interim daily dataset (Dee et al., 2011) is also extracted and used in our analysis. Here, the temperature profile is used to identify supercooled water clouds from all water clouds, determine the aerosol and cloud layer top temperatures, and calculate the lower-tropospheric static stability (LTSS), which is defined as the difference in potential temperature between 700 hPa and the surface (Klein and Hartmann, 1993), or $\Delta\theta = T_{700}\left(\frac{1000}{p_{700}}\right)^{R/C_p} - T_{sfc}\left(\frac{1000}{p_{sfc}}\right)^{R/C_p}$, where p is pressure, T is temperature, R is the gas constant of air, and C_p is the specific heat capacity at a constant pressure. A high LTSS value represents a stable atmosphere, whereas a low LTSS value represents an unstable atmosphere. In Section 3.4, we will discuss the effects of vertical velocity, LTSS and skin temperature on cloud phase in detail.

2.2 Cloud phase product

Naud et al. (2006) have indicated that cloud–radiation interactions are most sensitive to various parameters near the cloud top. Thus, we focus on the cloud top phase (CTP) and temperature (CTT) information in this analysis. Cloud phase information is derived from the CloudSat 2B-CLDCLASS-LIDAR (version 1.0) product. Compared with the CALIPSO phase identification (lidar-only alogorithm), the 2B-CLDCLASS-LIDAR product utilizes cloud boundaries retrieved from combined CPR and CALIOP measurements, the cloud layer maximum Ze identified with CPR, the layer integrated attenuated backscattering coefficient (IBC) from CALIOP and the temperature profile from the ECMWF-AUX product to identify three different cloud phases (ice, mixed and liquid). However, the Lidar-only phase algorithm only distinguishes the water and ice phases of a cloud by using the Lidar depolarization ratio and layer integrated attenuated backscattering coefficient (IBC) (Hu et al., 2007, 2009). Due to the strong multiple scatter effect in the Lidar depolarization measurements, as well as Lidar's limited ability to penetrate optically thick clouds, CALIPSO's Lidar-only algorithm is restricted in its ability to identify mixed-phase clouds; in particular, it is unable to penetrate the supercooled liquid layer to detect the ice layer (Zhang et al., 2010), and it is unable to distinguish pure liquid clouds from mixed-phase clouds. Nevertheless, only cloud top information is needed in this study. Therefore, the differences between these two algorithms should not result in abrupt or obvious changes in cloud phase fractions. Given the importance of multilayered cloud systems (Huang et al., 2005, 2006a; Lv et al., 2015), we obtain the cloud phase information of every cloud layer in each sample profile and further group every cloud layer into separate temperature bins (1ºC interval) according to the ECMWF-AUX temperature profiles and 2B-CLDCLASS-LIDAR cloud layer top heights. For mixed-phase clouds, we define the cloud as ice-topped or liquid-topped based on the "water_layer_top" information. If the temperature of the water layer in a mixed-phase cloud is equal to or lower than the mixed-phase cloud top temperature, it is classified as a liquid-topped cloud. Otherwise, it is classified as ice-topped. Furthermore, liquid phase clouds are divided into warm water-phase (CTT≥0) and supercooled water-phase (CTT<0) according to their cloud top temperature. Only

Atmos. Chem. Phys. Discuss., doi:10.5194/acp-2016-147, 2016
Manuscript under review for journal Atmos. Chem. Phys.
Published: 25 February 2016

those supercooled water phase clouds with a CTT between -40ºC and 0º C are further analyzed in this study. Here, we define the supercooled water cloud fraction (SCF) in a given temperature bin as the ratio of the number of liquid phase samples and the total (liquid+ice) samples gathered in a $2^{\circ}\times6^{\circ}$ grid box.

2.3 Aerosol types and relative frequency

Aerosol data are obtained from the CALIPSO level 2, 5 km aerosol layer product. Using scene classification algorithms (SCA), CALIPSO first classifies the atmospheric feature layer as either a cloud or aerosol by using the mean attenuated backscatter coefficients at 532/1064 nm, along with the color ratio (Liu et al., 2009). A confidence level for each feature layer is also reported in the level 2 products. Using the surface type, lidar depolarization ratio, integrated attenuated backscattering coefficient and layer elevation, aerosols are further distinguished as desert dust, smoke, polluted dust, clean continental aerosol, polluted continental aerosol, and marine aerosol (Omar et al., 2009). Mielonen et al. (2009) have used a series of Sun Photometers from the Aerosol Robotic Network (AERONET) to compare CALIOP and AERONET aerosol types and have found that 70% of the aerosol types from these two datasets are similar, with the closest similarities occurring in dust and polluted dust types. Mineral dust from arid regions has been widely recognized as an important source of ice nuclei in mixed-phase clouds because of its nucleation efficiency and abundance in the atmosphere (Richardson et al., 2007; DeMott et al., 2010; Atkinson et al., 2013). In addition to dust, some studies have also verified the potential ice nucleation ability of polluted dust and smoke at cold temperatures (Niedermeier et al., 2011; Cziczo et al., 2013; Zhang et al., 2015). For example, by using satellite lidar observations, Tan et al (2014) have found negative temporal and spatial correlations between the supercooled liquid cloud fraction and the polluted dust and smoke aerosol frequencies at the −10ºC, −15ºC, −20ºC, and −25ºC isotherms, although those correlations are weaker than those found between dust frequencies and the supercooled liquid cloud fraction. As a result, we combine the dust, polluted dust and smoke information from CALIPSO to further analyze the relationship between aerosols and the SCF in this study. Given the difficulty of quantifying the concentration of IN aerosols (here, IN aerosols are the sum of dust, polluted dust and smoke), this study utilizes the relative occurrence frequency of IN aerosols to quantify this variable instead. We first group every IN aerosol sample from each observation profile into a different temperature bin (1ºC interval) according to the ECMWF-AUX temperature profiles and CALIPSO aerosol layer top height measurements. Then, following Choi et al. (2010), we define the frequency of IN aerosols within a given temperature bin as the ratio of the number of IN aerosol samples to the total number of observation profiles in the same temperature bin and grid. Finally, we calculate the relative occurrence frequency of IN aerosols with respect to the highest IN aerosol frequency. The relative occurrence frequency of aerosols is indicative of the temporal and spatial variability of IN aerosols compared to the maximum occurrence frequency (Choi et al., 2010). We remove those aerosol layers with low confidence values (that is, those with an absolute value lower than 50) from the dataset (approximately 6.5% of all aerosol layers).

3. Results

3.1 Cloud phase partitioning schemes in GCMs

Recently, several ice nucleation processes based on theoretical and empirical studies have been developed to more explicitly represent these processes in certain climate models. These new schemes have indicated that the liquid cloud fraction should depend not only on temperature but also on the presence of aerosols that have undergone ice nucleation (Storelvmo et al., 2008; Gettelman et al., 2012). However, many models still specify the liquid-phase cloud fraction solely as a function of temperature (Doutriaux-Boucher and Quaas, 2004; Hu et al., 2010; Song et al., 2012) because the microphysical and dynamic processes of cloud formation are not yet fully understood. For example, Choi et al. (2014) have summarized the cloud phase partitioning schemes used in various climate models and have studied the influence of cloud phase composition on climate feedbacks. They outlined the two cloud phase schemes that are widely used in present models. Scheme 1 can be written as:

Atmos. Chem. Phys. Discuss., doi:10.5194/acp-2016-147, 2016
Manuscript under review for journal Atmos. Chem. Phys.
Published: 25 February 2016

$$f = \left(\frac{T - T_{ice}}{T_w - T} \right)^n \qquad (1)$$

For scheme 2, the liquid fraction f can be expressed as:

$$f = \exp[-(\frac{T_w - T}{15})^n] \qquad (2)$$

where T is temperature, $T_{ice} \le T \le T_w$, T_w is the temperature above which all clouds are liquid, T_{ice} is the temperature below which all clouds are ice, and n is a shape parameter that controls the slope of $f(T)$ between -40º and 0º. Based on table 1 of Choi et al. (2014), we select several models and list the values of these parameters in Table 1. Obviously different thresholds of these parameters and different cloud phase schemes in climate models indicate that an inability for models to accurately separate the cloud phases, and the large biases and inconsistency between the models may be because these thresholds are based on aircraft observations or field experiments from different regions. Thus, a constant global threshold would probably introduce large uncertainty in the simulation of cloud feedbacks, and the spatial and temporal variations of these parameters should be considered in the future parameterization of cloud phase partitioning.

3.2 Global distributions of T_w, T_{ice} and n

Based on the processes outlined in Section 2.2, the SCF for each temperature bin (1K) of every grid can be derived. The value of T_w in each grid equals the temperature above which all SCFs equal 1, whereas the value of T_{ice} in each grid equals the temperature below which all SCFs equal 0. After obtaining values for T_{ice} and T_w, the value of n can be further determined by performing nonlinear fitting to T_{ice}, T_w, f and T using Eq.(1). In the following analysis, we determine that scheme 1 (Eq. (1)) better simulates the variation of SCF with temperature than scheme 2 (Eq. (2)), and thus only the distributions of n for scheme 1 are provided in this section.

Fig. 1 shows the geographic and seasonal variations of T_w values across the $2^{\circ}\times6^{\circ}$ grid boxes based on the 2B-CLDCLASS-LIDAR product. The gaps (no color) indicate missing data or areas where the supercooled water cloud fraction doesn't reach 1 between -40 ºC and 0 ºC. Those grids in which T_w is higher than 0 ºC are excluded in this study. These grids almost all located within typical subsidence regions (e.g., stratocumulus regions) where strong subsidence favors low cloud formation and suppresses ice or mixed-phase cloud generation (Yuan and Oreopoulos, 2013). Fig. 1 clearly illustrates that the value of T_w ranges from -2ºC to -6ºC across the majority of the globe; moreover, no clear seasonal variations are found in our results for T_w. At high latitudes, T_w ranges from -2ºC to -3ºC; this value decreases from the high latitudes to the tropics. Our analysis indicates that the current T_w value used in CAM3 may be too low and may result in the overestimation of supercooled water clouds at lower altitudes (see Fig. 7), whereas the T_w value used in CAM5 is consistent with the distribution of T_w for most regions across the globe. For the ERA40 reanalysis dataset (Weidle and Wernli, 2008) and other models such as the LMDZ (Doutriaux-Boucher and Quaas, 2004), a high threshold is generally adopted, which probably results in the underestimation of supercooled water clouds at lower altitudes. Fig. 2 illustrates the geographic and seasonal variations of T_{ice} at the $2^{\circ}\times 6^{\circ}$ grid box scale. The warmest T_{ice} values for each season generally occurs in typical stratocumulus regions and in northern Africa; these values are warmer than -26ºC, indicating that supercooled water clouds in these regions are restricted to warmer atmospheric levels than are found throughout the majority of the world, where T_{ice} values are almost always below -30ºC. Although the differences between these observations and the models are clear, the thresholds used in the CAM3 (or 5) cloud phase scheme and GISS are relatively reasonable compared with those values used in the ERA40 reanalysis dataset (Weidle and Wernli, 2008) and other models. Generally, T_{ice} values can reach lower temperatures in a clean or IN-poor environment. However, our results show that the geographic and seasonal variations in T_{ice} are also negligible under different aerosol loading conditions, indicating that the combination of several factors, such as IN, vertical motion or other dynamic parameters affect the distribution of T_{ice}.

In each model's cloud phase scheme, the shape parameter n controls the slope of the curve between temperature and the supercooled water cloud fraction. For example, in scheme 1, a large n value corresponds to a low liquid cloud fraction at a given

Atmos. Chem. Phys. Discuss., doi:10.5194/acp-2016-147, 2016
Manuscript under review for journal Atmos. Chem. Phys.
Published: 25 February 2016

cloud top temperature T, T_{ice}, and T_w. This relationship is showed in Fig. 3, which depicts the apparent decreases of grid-mean SCF from 0.6 to 0.3 with corresponding increases in parameter n from 0.5 to 5.5. Here, the grid-mean SCF is the averaged value of the supercooled water cloud fraction from all cloud top temperature bins ranging from -40ºC to 0ºC within a given grid cell, and the color bar represents the number of grid cells within a 4 year period. Further, Fig. 4 shows the clear geographic and seasonal variations of parameter n. Based on Fig. 4, we find that n is approximately 1 at 60º poleward and varies strongly from 0 to 5 throughout a majority of the globe. Larger values (equal to or greater than 3) locate at the mid-latitudes of the northern hemisphere, South America and the mid-latitude oceans of the southern hemisphere. Especially at the mid-latitudes of the northern hemisphere, the value reaches even 4 or 5. Given the values of n used in the CAM 3 (Collins et al., 2004) and CAM 5 (Song et al., 2012), it is clear that the CAM 3 and CAM5 better simulate the relationship between temperature and SCF at the high-latitudes (60º poleward); meanwhile, the values of n adopted in the ERA40 (Weidle and Wernli, 2008) and LMDZ (modified version) (Doutriaux-Boucher and Quaas, 2004) are consistent with observed results in only some regions during certain seasons (e.g., the Pacific Ocean during all seasons except summer, and the high-latitudes of the northern hemisphere during summer and Russia year-round). For other regions such as Asia, South America and the North Pacific, large n values in these models definitively indicate the models' inability to accurately simulate the relationship between temperature and SCF locally.

3.3 Evaluation of cloud phase partitioning schemes

Following the process used to evaluate scheme 1, we also derive the parameter n for scheme 2 (not shown). After inputting the dynamic thresholds of T_{ice}, T_w and n into Eq. (1) and Eq. (2), we are able to calculate the SCF of each cloud top temperature bin within each geographic grid for the different schemes, and we further evaluate which scheme is better able to simulate the variation of SCF with temperature in each grid. Here, we define the grid mean absolute value of the difference between calculated and observed SCF (absolute difference) at each temperature bin as follows:

Atmos. Chem. Phys. Discuss., doi:10.5194/acp-2016-147, 2016
Manuscript under review for journal Atmos. Chem. Phys.
Published: 25 February 2016

Atmospheric Chemistry and Physics
Discussions

$$Abs\_dif = \sum_{T=-40^{o}C}^{0^{o}C} |SCF^{T}_{calculated} - SCF^{T}_{observed}| \Big/ 41 \tag{3}$$

Following the same logic, the grid mean relative difference can be written as:

$$\mathrm{Re}\_dif = \sum_{T=-40^{o}C}^{0^{o}C} (SCF^{T}_{calculated} - SCF^{T}_{observed}) \Big/ 41 \tag{4}$$

where T is the cloud top temperature, and $SCF^{T}_{observed}$ and $SCF^{T}_{calculated}$ are the observed and calculated SCFs from scheme 1 and 2, which are determined by inputting the dynamic (or fixed) thresholds of T_{ice}, T_{w} and n into Eq. (1) and Eq.(2), respectively. In addition, 41 is the number of cloud top temperature bins from -40ºC to 0ºC. Figs. 5 and 6 compare the geographic distributions of absolute and relative differences (annual means) for different schemes, respectively. Compared with scheme 2, which is used in the GISS model (see Fig. 5b), the cloud phase partitioning scheme (scheme 1) is used in CAM 3 (or 5) better simulate the variation of SCF with temperature almost everywhere, especially at the mid- and high-latitudes (see Fig. 5a). For example, the absolute difference for scheme 1 (Fig. 5a) is smaller than 0.08 at 40º poleward, with a large value (0.12) only apparent in the oceanic regions of the subtropics. However, in scheme 2 (Fig. 5b), the differences across most regions of globe still exceed 0.16, even when dynamic thresholds are inputted. Figs. 5c and 5d further illustrate the absolute difference between CAM3 (and 5) calculated SCFs and observed SCFs. At present, CAM 3 and CAM 5 still rely on unique temperature thresholds and the n value identified in scheme 1 for the entire globe, which has led to considerable variations in absolute difference values compared with those shown in Fig. 5a. By comparing Figs. 5b and 5d, we find that the distributions and magnitudes of the absolute differences are very similar, and even the high-latitude values from CAM5 are smaller than those results derived from scheme 2. These figures further verify the importance of the cloud phase partitioning scheme in general circulation models. Although the schemes used in CAM 3 and 5 are similar, the difference is more apparent in CAM 3 than CAM 5 (see Fig. 5c). In fact, based on Eq.(1) and Table 1, it is clear that the difference between Fig. 5c and 5d is mainly caused by the unreasonable threshold of T_{ice} in the CAM3, which yields an additional 17% difference in values compared to the CAM5. However, the limits of CAM 5 are still apparent in the northern hemisphere, as seen by comparison of Figs. 5a and 5d, especially at mid-latitudes where the effect of IN aerosols is important (the difference can reach 0.2). Thus, scheme 1's ability to consider the dynamic thresholds of T_{ice}, T_w and n may further improve the prediction of the supercooled water cloud fraction at different temperatures, particularly poleward of 40°, thus making it a preferred option in general circulation models. For relative difference values (Fig. 6), a clear underestimation (exceeding -6%) occurs poleward of 60°S over the ocean (Figs. 6b and 6d), whereas SCF is overestimated significantly (14%) in other regions by the models, especially CAM 3 (Fig. 6c). However, the relative difference for scheme 1, which consider the dynamic thresholds of T_{ice}, T_w and n, ranges from only -0.04 to 0.02 (Fig. 6a).

For studying the vertical distribution of zonal mean SCF with temperature, and further evaluating the absolute and relative differences between calculated and observed SCFs for scheme 1 are mainly from which temperature bin, the Fig. 7 give us some new insights. For example, Fig.7a depicts the vertical distribution of zonal mean SCFs (annual mean) with temperature based on the observation. Here, the SCF at each temperature bin of each latitude belt is the averaged value of SCFs of all grids at this temperature in this latitude belt. Fig. 7a further illustrates that nearly all of the SCF values are close to 1 or 0 at temperatures above -5ºC and below -35ºC, respectively. Thus, the T_{ice} and T_w temperature thresholds used in CAM5 are probably more reasonable values than those in CAM3, at least at the zonal mean level. In addition, the meridional asymmetry (or hemispheric asymmetry) of the SCF values is apparent, with southern hemispheric values exceeding those in the northern hemisphere. This clear difference is particularly prominent at the temperature range from -15ºC to -30ºC poleward of 50°S, where the difference between SCFs in the southern and northern hemispheres sometimes exceeds 20% and reaches 40% at -25ºC in the polar region (figure not shown). Given the similar vertical distributions of the SCF values, Fig. 7b provides a typical example of the SCF profile differences

Atmos. Chem. Phys. Discuss., doi:10.5194/acp-2016-147, 2016
Manuscript under review for journal Atmos. Chem. Phys.
Published: 25 February 2016

between the dynamic thresholds derived by scheme 1 and the observed values. Overall, the difference is small in most temperature bins (with bias ranging from -9% to 9%) and is primarily concentrated in the southern hemisphere. A clear underestimation (or overestimation) exceeding 12% is produced by scheme 1 for the temperature range -20ºC to -25ºC (or about -10ºC) at 40°S to 40°N, and especially approximately 40°S; however, CAM3 generally produces a substantial overestimation almost everywhere except for the temperature range -20ºC to -25ºC poleward of 60°S, where a slight underestimation occurs (from 9% to18%). The significant overestimation of SCF by CAM3 is particularly prominent in the lower atmosphere at temperatures between -10ºC to -20ºC for almost every latitude belt (where the bias reaches up to 45%). For those regions where temperatures drops below -20ºC, the SCF bias decreases to approximately 30%; nevertheless, SCF values are still significantly overestimated. Compared with CAM3, the bias is smaller in CAM5 (Fig. 7d), although the patterns of differences are very similar. At the temperature range -20ºC to -25ºC poleward of 60°S, the underestimation of values (approximately 30%) is more apparent than those results for the same range derived from CAM3. Fig. 6 allows us to infer that the clear bias in relative differences poleward of 60°S produced by CAM5 is primarily caused by the underestimation of SCFs in the -20ºC to -25ºC temperature range, whereas the apparent overestimation of SCF from -10ºC to -20ºC contributes most of the bias at other latitude belts.

3.4 Effects of atmospheric dynamics and aerosols on cloud thermodynamic phase

The above analysis demonstrate the inability of current models to accurately simulate the vertical and geographic variations of the supercooled cloud fraction, due to incomplete knowledge of the underlying physical processes related to cloud phases. In fact, several factors in addition to cloud top temperature, including IN and vertical motion, probably together affect the distribution of the supercooled cloud fraction, especially the relationship between temperature and supercooled water clouds. For example, the distribution of parameter *n* at the mid-latitudes of the northern hemisphere may be largely related to dust aerosols that can serve as IN and thus enhance the glaciation occurrences at lower relative SCFs than in other regions of the

Atmos. Chem. Phys. Discuss., doi:10.5194/acp-2016-147, 2016
Manuscript under review for journal Atmos. Chem. Phys.
Published: 25 February 2016

globe at a given cloud top temperature, e.g., -20ºC (Fig. 8). For example, as showed in Fig. 8, the SCF at -20ºC is only approximately 0.12 (especially at spring) at the mid-latitudes of the northern hemisphere, whereas SCF reaches 0.7 at the high-latitudes of the southern hemisphere (that is, poleward of 60°S). Our results are consistent with those from previous studies from Choi et al (2010) and Tan et al (2014), which have verified that the regional differences in the supercooled water cloud fraction at -20ºC are highly correlated with the dust frequency above the freezing level. However, by collocating this variable with the geographic and seasonal distributions of relative aerosol occurrence frequency (RAOF) at -20ºC (see Fig. 9), we find that the SCF still has a low value at the mid-latitudes of the northern hemisphere during the summer season, even though the IN aerosol loading is insignificant at -20ºC in these regions. As in the findings of Choi et al (2010), our results also show that the persistent low SCF (or large *n*) throughout the year at −20ºC (see Fig. 8) could not be explicitly related to IN aerosol frequency because the RAOF is significantly lower in central South America. These results indicate that aerosols' effect on nucleation cannot fully explain all changes of cold cloud phase in our study; In other words, there is no evidence to suggest that its effect is always dominant at each altitude of each region.

Besides aerosol effect, what is the role of meteorological effect in determining cloud phase change, especially at those regions which aerosol effect on nucleation isn't a first-order influence due to low IN aerosol frequency To further discuss this question, we analyze the seasonal and zonal variations of SCF and RAOF at -20ºC, LTSS and 500 hPa vertical velocity (see Fig. 10). For the tropical region (from 20°S to 20°N), the RAOF is very low (approximately 0.005) and the seasonal variation is negligible. However, the corresponding SCF undergo a clear seasonal change. For example, opposing SCF distributions are found during the summer and winter, and the maximum difference reached 15%. Opposite distributions are primarily linked to distinctly different atmospheric vertical motions, whereas surface temperature (figure not show) and LTSS contribute minimal amounts, due to their weak seasonal variation above this region. During the summer, the inter-tropical convergence zone (ITCZ) is

Atmos. Chem. Phys. Discuss., doi:10.5194/acp-2016-147, 2016
Manuscript under review for journal Atmos. Chem. Phys.
Published: 25 February 2016

correlated with deep convective clouds shift to the northern hemisphere and has strong vertical velocity. In contrast, the strength of atmospheric vertical motion in the northern hemisphere tropics decreases during the winter season, due to the ITCZ shift to the southern hemisphere. Poleward of 40°N, the inconsistency of seasonal variations in SCF and RAOF is particularly apparent. For example, maximum RAOF and SCF are visible during winter at the middle and high latitudes of the northern hemisphere, whereas these values both decrease during the summer. Another apparent phenomenon is that winter RAOF values are larger than spring values poleward of 40°N. We recalculate the RAOF by considering only IN dust aerosols, and find that this phenomenon still exists. These results suggest that the trend is real and is not fully caused by combined polluted dust and smoke frequencies, thus verifying the importance of meteorological effects on cloud phase changes. Figs. 10a and 10b show how the differences between winter and summer SCF may be linked to the seasonal variations in surface temperature and atmospheric stability (LTSS), whereas seasonal changes in vertical motion are weak and probably minimally affect SCF at the mid- and high-latitudes of the northern hemisphere. The results also show that the effects of different meteorological factors on cold cloud phase have regional characteristics. That is, low surface temperature and high LTSS (or a stable atmosphere) inhibit ice nucleation and push supercooled water to colder temperatures at mid- and high-latitudes, whereas strong vertical motion enhances ice nucleation in the tropics.

To further quantify the effects of aerosol and meteorological factors on cold cloud phase, we group the RAOFs of grids into several RAOF bins within each specified vertical velocity, surface temperature or LTSS bin in order to analyze the relationship between the studied parameters (SCF at -20ºC, T_{50} and n) and aerosol loading under different meteorological conditions. Here, T_{50} is defined as the cloud top temperature for exactly 50% of supercooled water clouds (Naud et al. 2006) and can be derived by inputting the T_{ice}, T_w, n and f (50%) thresholds into Eq. (1). Fig. 11 gives the seasonal and geographic variations of this parameter. Based on Fig. 11, we find that T_{50} in the high-latitude regions is lower (around -20ºC) than that in other regions, especially the middle latitudes of the two hemispheres, where T_{50} reaches -10ºC. The apparent difference (approximately 10K) in T_{50} values between the high and middle latitudes reflects the general tendency for supercooled water clouds to persist at colder temperatures in the high latitude regions, and this result based on global observation also further supports the findings of Naud et al. (2006), who have analyzed MODIS data collected over the North Atlantic and Pacific Ocean basins. Naud et al. (2006) have also found that the warmest T_{50} values in each studied subregion generally occur in areas of ascent and heavy precipitation. However, by analyzing the distributions of T_{50} on a global scale, our results indicate that strong subsidence areas also tend to generate warm T_{50} values. This phenomenon is particularly apparent in Fig. 12, which depicts the dependences of T_{50}, n and SCF on the RAOF and 500 hPa vertical velocity. Notably, the temperature bins used to calculate the RAOF differ for T_{50}, n and SCF, based on their global distributions (See Fig. 4, Fig. 8 and Fig. 11). For example, parameter n reflects the relationship between SCF and CTT at the temperature ranges from -40ºC to 0ºC; thus, the calculation of RAOF for n considers aerosols at all temperature bins from -40ºC to 0ºC. However, only the aerosol samples at ±2 bins around -20ºC are used to calculate the RAOF for SCF at -20ºC. For T_{50}, the calculation of RAOF is primarily based on aerosol samples from the -20ºC to 0ºC temperature bins. We separate the relationship between T_{50} and RAOF into three groups based on the strength of the 500 hPa vertical velocity (e.g., 0<|vertical velocity|<=25 hPa/day, 25<|vertical velocity|<=50 hPa/day and |vertical velocity|>50 hPa/day). Such grouping ensures a sufficient number of samples available in each bin (at least hundreds of samples in each bin) to ensure statistical significance. The error bars correspond to the ±5 standard error. Here, the standard error (SE) is computed as: $SE = SD/\sqrt{N}$, where SD is the standard deviation of the data falling in an RAOF bin and vertical velocity bin, and N is the sample number in each bin. As RAOF increases (Fig. 12a), T_{50} gradually tends to increase from around -20ºC (IN aerosols absent) to approximately -12ºC (high aerosol loading). The continuously increasing trend verifies that the existence of IN aerosols can hasten the glaciation of supercooled droplets through the Bergeron-Findeisen growth mechanism of ice crystals (e.g., Pruppacher and Klett, 1978). The value of T_{50} tends to increase when the 500 hPa vertical velocity increases from <25 hPa/day to >50 hPa/day. That is, strong vertical velocity can also force supercooled water to glaciate at a warmer temperature. On average, the maximum difference in T_{50} with and without aerosol loading reaches 8K, whereas the effects of different vertical velocities result in a difference of approximately 2K within the same RAOF bin. This result indicates that the effect of vertical motion on T_{50} is relatively smaller than the effect of aerosols. Based on the MODIS retrieval data, Naud et al. (2006) have analyzed the frontal ascent region of storm systems. They have found that glaciation occurs on average at the warmest temperature (warm T_{50}), where the strongest precipitation rates and updrafts occur. In addition, a vigorous ascent may maintain conditions near water saturation, and T_{50} values close to those at which the Bergeron-Findeisen process operates most efficiently may indicate that the process limits the existence of liquid droplets at colder temperatures.

Fig. 12b illustrates the relationships between parameter n and aerosol loading for different vertical velocities. As with Fig. 12a, the n value gradually increases as RAOF increases, and those regions with a large vertical velocity have large n values. On average, the maximum difference in n values for areas with and without IN aerosol loading is approximately 2, and the n bias caused by vertical motion is relatively less than (approximately 0.5) than the aerosol effect. Large n values correspond to small SCF values, and Fig. 12c clearly shows the decreasing tendency of SCF at -20ºC as the RAOF and 500 hPa vertical velocity increase. The logarithmic intervals of RAOF (see the X-axis of Fig. 12c) indicate that there is a semi-logarithmic relationship between SCF and RAOF (Choi et al., 2010). For relatively clean air without IN aerosols, the SCF at a cloud top temperature of -20 ºC exceeds 40% when the 500 hPa vertical velocity is smaller than 25 hPa/day. This value gradually decreases to 15% under high aerosol loading conditions when the 500 hPa velocity is also high (>50 hPa/day). The clearly decreasing trend in SCF with increasing RAOF is concordant with previous studies' conclusions based on CALIPSO measurements (Choi et al., 2010; Tan et al., 2014). These distinctly

Atmos. Chem. Phys. Discuss., doi:10.5194/acp-2016-147, 2016
Manuscript under review for journal Atmos. Chem. Phys.
Published: 25 February 2016

separate curves verify that the vertical velocity indeed significantly affects ice nucleation even in the case of high aerosol loading. In fact, the effect is particularly important in those regions without IN aerosols where the SCF bias can reach 15%, such as in the tropics. For the same RAOF bin, a large vertical velocity can enhance the glaciation process and reduce the SCF, which partly explains why the persistent low SCF at -20ºC across central South America throughout the year could not be explicitly related to aerosol frequency. Overall, different vertical motions lead to 10% mean SCF differences, and the bias is comparable to the effect of aerosols on cloud phase changes when the vertical velocity is limited to the same speed.

Similarly, Figs. 13 and 14 show how T_{50}, n and SCF depend on aerosols, surface temperature and atmospheric stability, respectively. Here, surface temperature is classified into three levels: high, where the surface temperature≥285 K; medium, where 270 K≤surface temperature<285 K; and low, where surface temperature<270K. Generally, high surface temperatures enhance ice nucleation and reduce SCF values (or have large n values). As with strong vertical velocity, warm surface temperatures can also force supercooled water to glaciate at warmer temperatures. The difference in T_{50} values at different surface temperatures reaches 10K without aerosol loading and gradually decreases to approximately 3K with high aerosol loading. On average, the different surface temperatures lead to 25% SCF differences, and the bias is larger than the difference caused by different vertical motions (10%). This is also comparable to the effect of aerosols on cloud phase changes when the vertical velocity is limited to the same level. High LTSS represents a stable atmosphere, whereas low LTSS represents an unstable atmosphere. In Fig. 14, a stable atmosphere (LTSS>=19K) can be seen to inhibit ice nucleation and enhance the SCF, and it is associated with colder T_{50} values than an unstable atmosphere (LTSS<=14K). Although the effects of LTSS on these parameters are not as apparent as those of surface temperature and vertical motion, some interesting results still are captured. Naud et al. (2006) have found that outside the frontal ascent zone, T_{50} is not uniformly warm everywhere the mean strength of the 500 hPa vertical velocity is high. They have suggested that vigorous updrafts either suppress ice formation or advect supercooled water to the colder cloud top level because vigorous updrafts do not leave enough time for supercooled droplets to glaciate as ice crystals (Bower et al., 1996). In fact, these two opposite mechanisms may correspond to storms of different intensities, different cloud systems within different atmospheric stability levels (convective cloud or stratiform frontal cloud) or different locations with the cloud (cloud top or inside the cloud) (Bower et al., 1996; Naud et al., 2006). In our results, we find that Naud's results outside the frontal ascent zone may be interpreted using the LTSS and surface temperature. For the same vertical motion, high LTSS tends to reduce the T_{50} to a cold temperature. In addition, stratiform clouds can be generated more easily within a stable atmosphere; thus, different LTSS values are linked to different cloud systems. Compared with a convective cloud system, which requires a warmer surface temperature and lower LTSS, stratiform clouds have a weak precipitation rate and inhibit the exhaustion of supercooled water. Thus, different T_{50} values within and beyond the frontal ascent zone for similar vertical motions in Naud et al. (2006) actually reflect different surface temperatures and LTSS. By performing a similar analysis at different latitudes, we further find that the effect of LTSS on cloud phase is obvious at middle and high latitudes, particularly in the northern hemisphere, where shallow stratiform clouds such as altostratus, stratus and nimbostratus clouds are frequent (Wang and Sassen, 2001; Sassen and Wang, 2008; Li et al., 2015). Due to the wide distribution of land at the middle and high latitudes of the northern hemisphere, seasonal variations in surface temperature result in significant differences in LTSS during different seasons, which further causes a difference in cloud types and amounts over this region. By comparing the different cloud types and covers at different seasons using the 2B-CLDCLASS-LIDAR, we find that shallow stratiform cloud covers such as, altostratus, stratus and nimbostratus clouds indeed are greater during winter than summer, providing a reason for why the SCF and RAOF are both larger during the winter than the summer.

In the cloud phase partitioning schemes of models, we primarily focus on the effects of aerosols and dynamic factors on the parameter n. However, we also perform a similar analysis for T_w with n, and we find that the value of T_w systematically

Atmos. Chem. Phys. Discuss., doi:10.5194/acp-2016-147, 2016
Manuscript under review for journal Atmos. Chem. Phys.
Published: 25 February 2016

increases with increases in IN aerosols from -9ºC to -4ºC, indicating that high aerosol loading can enhance the temperature of glaciation. However, the effect of dynamic factors on T_w is negligible. In addition, the stable relationship between aerosols (or dynamics) and T_{ice} is not evident in our results, indicating the complexity of the distribution of T_{ice}. Based on the above analysis, the current model (e.g., CAM5) already provides relatively reasonable T_{ice} and T_w values compared with other models. Its bias toward SCF is primarily caused by the unreasonable presentation of parameter *n*, which is closely linked to aerosol loading and meteorological factors. These results thus suggest that the effects of dynamics and aerosols on the parameters (especially for parameter *n*) in the studied cloud phase partitioning schemes are very important and should be considered in the parameterization of cloud phase in future studies in order to further improve the calculation of cloud radiative effects related to cloud phase changes.

4. Conclusions and Discussion

Changes in cloud phase can significantly affect the Earth's radiation budget and global hydrological cycle (Sassen and Khvorostyanov, 2007; Choi et al., 2010). Based on 4 years (2007–2010) of cloud phase data and aerosol products from CloudSat and CALIPSO, as well as meteorological parameters from the ECMWF-AUX and ERA-Interim products, this study investigate the effects of atmospheric dynamics and aerosols on the thermodynamic phase of cold clouds on a global scale. Although some statistical results reasonably agree with previous research, new insights are also achieved in this paper.

For certain current GCMs, unique temperature thresholds (for T_{ice} and T_w) and relationships (for parameter *n*) are used in the models' cloud phase partitioning schemes, regardless of their geographic or temporal variations, which may result in considerable differences regarding the estimation of the supercooled liquid cloud fraction at a given cloud top temperature between the GCMs. By using the observations from space lidar and radar, we find that the value of T_w ranges from -2ºC to -6ºC across most regions of the globe; moreover, there is no clear seasonal variation in our results for T_w. At the high-latitudes, T_w ranges from -2ºC to -3ºC; this value decreases from high latitudes to the tropics. T_{ice}, is warmer (>-26ºC) in typical stratocumulus regions and northern Africa when compared to values across the rest of the world, where T_{ice} is almost exclusively below -30ºC. These results verify the reasonableness of thresholds in CAM5 compared to other models, which may overestimate (or underestimate) supercooled water clouds at lower atmospheric levels on the basis of the T_w threshold used. The geographic and seasonal distributions of parameter n are closely linked to aerosol loading and meteorological parameters (e.g., vertical velocity, LTSS and surface temperature). Our results indicate that the value of n varies strongly from 0 to 5 across the majority of the globe. High values (equal to or greater than 3) occur at the mid-latitudes of the northern hemisphere, South America and the mid-latitude oceans of the southern hemisphere. Values of n in the CAM3 and CAM5 models best illustrate the relationship between temperature and SCF at the high-latitudes (60º poleward). By comparing the absolute and relative differences between different cloud phase schemes and remote-sensing observations, we suggest that scheme 1 used in CAM3 and CAM5 is a preferred option in the models, and the application of dynamic T_{ice}, T_w and n thresholds should further improve the predictions of the supercooled water cloud fraction for different temperatures, particularly over the region poleward of 40°.

To clarify the roles of meteorological factors and aerosol loading in determining cloud phase changes and further provide observational evidence for the design and evaluation of a more physically based cloud phase partitioning scheme, we perform a series of analyses that investigate the effects of atmospheric dynamics and aerosols on the thermodynamic phase of clouds on a global scale. Statistical results indicate that aerosols' effect on nucleation can't fully explain all cold cloud phase changes, especially in those regions where aerosols' effect on nucleation is not a first-order influence (e.g., due to low IN aerosol frequency). As with the effects of IN aerosols, we find that strong vertical motion enhances the glaciation process, reduces the SCF (or increases the n value), and forces the supercooled water to glaciate at a warmer temperature. For the same vertical motion, however, high LTSS (or low surface temperature) tends to increase the SCF and force the supercooled water to glaciate at a colder temperature. These two opposite mechanisms may correspond to different cloud systems (e.g., convective clouds or stratiform frontal clouds) or to different precipitation intensities. An unstable atmosphere (low LTSS and high surface temperature) in those strong ascent regions favors the formation of deep convective clouds and exhausts the supply of supercooled water through a strong precipitation rate. A stable atmosphere (high LTSS and low surface temperature) favors the formation of shallow stratiform clouds and can inhibit the exhaustion the supercooled water via a weak precipitation rate. These results are consistent with partial findings from previous studies (Naud et al., 2006; Choi et al., 2010) and may help in interpreting some confusing phenomena observed in previous and our studies (Choi et al., 2010). For example, these results explain why the values of SCF and RAOF during the winter are both larger than values obtained during the summer at the middle and high latitudes of the northern hemisphere.

Previous studies have mainly focused on warm water cloud systems (Li et al., 2011, 2013; Kawamoto and Suzuki, 2012, 2013) or dust properties retrieval and simulations (Huang et al., 2010; Bi et al., 2011; Liu et al., 2011; Chen et al., 2013) or have demonstrated the importance of dust on cloud properties (Huang et al., 2006b, 2006c, 2014; Su et al., 2008; Wang et al., 2010). However, systematic studies on the statistical relationship between cold cloud phase (in particular, supercooled water clouds) and IN aerosol properties under different dynamic conditions on a global scale have received far less attention. Our results, which are based on global observations, verify the effects of dynamic factors on cloud phase changes and illustrate that these effects are regional, thus suggesting potential implications for further improving the parameterization of cloud phases and determining the climate feedbacks. General circulation model (GCM)-simulated storm tracks move poleward (Yin, 2005), as do the associated water clouds. The difference in albedo feedback among different models is primarily a result of the differences in the poleward redistribution of cloud-based liquid water and is related to differences in mixed-phase cloud algorithms (Tsushima at al., 2006): those models that produce more supercooled water clouds have a higher sensitivity. However, with global warming, a number of studies have shown that spring dust storm frequencies negatively correlate with local surface air temperatures and have shown a downward trend over the past 50 years (Qian et al., 2002; Zhu et al., 2008). In addition, the warming of surface temperatures in recent decades has been enhanced relative to mean global warming by approximately 50% in the United States, a factor of 2–3 in Eurasia, and a factor of 3–4 in the Arctic and the Antarctic Peninsula (Hansen et al., 2010). It is uncertain how these trends will affect cloud phase changes and whether more ice or more supercooled water will occur. To answer this question, our results suggest that the effects of dynamic factors on cloud phase changes should be considered in the parameterization of cloud phases within GCMs in order to further reduce the biases of climate feedbacks and climate sensitivity among these models.

Acknowledgments.
This research was jointly supported by the key Program of the National Natural Science Foundation of China (41430425), Foundation for Innovative Research Groups of the National Science Foundation of China (Grant No. 41521004), National Science Foundation of China (Grant No. 41575015 and 41205015) and the China 111 project (No. B13045). We would like to thank the CALIPSO, CloudSat and ERA-Interim science teams for providing excellent and accessible data products that made this study possible.

References

Atkinson, J. D., Murray, B. J., Woodhouse, M. T., et al.: The importance of feldspar for ice nucleation by mineral dust in mixed-phase clouds, Nature, 498, 355-358, 2013.

Bi J., Huang, J., Fu, Q., Wang, X., Shi, J., Zhang, W., Huang, Z., and Zhang, B.: Toward characterization of the aerosol optical properties over Loess Plateau of Northwestern China, J. Quant. Spectrosc. Radiat. Transf., 112, D00K17, doi:10.1029/2009JD013372, 2011.

Bower, K. N., Moss, S. J., Johnson, D.W., Choularton, T.W., Latham, J., Brown, P. R. A., Blyth, A.M., and Cardwell, J.: A parameterization of the ice water content observed in frontal and convective clouds, Quart. J. Roy. Meteor. Soc., 122, 1815–1844, 1996.

Chen, S., Huang, J., Zhao, C., Qian, Y., Leung, R., and Yang, B.: Modeling the transport and radiative forcing of Taklimakan dust over the Tibetan Plateau: A case study in the summer of 2006, J. Geophys. Res., 118, doi:10.1002/jgrd.50122, 2013.

Cheng, A., Xu, K.M., Hu, Y., and Kato, S.: Impact of a cloud thermodynamic phase parameterization based on CALIPSO observations on climate simulation, J. Geophys. Res., 117, D09103, doi:10.1029/2011JD017263, 2012.

Choi, Y.S., Lindzen, R.S., Ho, C.H., and Kim, J.: Space observations of cold-cloud phase change, Proc. Natl. Acad. Sci. U.S.A., 107, 11, 211–11,216, 2010.

Choi, Y.S., Ho, C.H., Park, C.E., Storelvmo, T., and Tan, I.: Influence of cloud phase composition on climate feedbacks, J. Geophys. Res. Atmos., 119, 3687–3700, doi:10.1002/ 2013JD020582, 2014.

Collins, W. D., et al.: Description of the NCAR Community Atmosphere Model (CAM 3.0), National Center for Atmospheric Research, Boulder, Colo, 2004.

Cziczo, D.J., Froyd, K.D., Hoose, C., Jensen, E.J., Diao, M., Zondlo, M.A., Smith, J.B., Twohy, C.H., and Murphy, D.M.: Clarifying the dominant sources and mechanisms of cirrus cloud formation, Science, 340(6138), 1320–1324, doi:10.1126/science.1234145, 2013.

Dee, D.P., Uppala, S.M., Simmons, A.J., et al.: The ERA‐Interim reanalysis: Configuration and performance of the data assimilation system, Quart. J. Roy. Meteor. Soc., 137(656), 553-597, 2011.

Del Genio, A.D., Yao, M.S., Kovari, W., and Lo, K.W.: A prognostic cloud water parameterization for global climate models, J. Clim., 9, 270–304, 1996.

DeMott, P.J., Prenni, A.J., Liu, X., et al.: Predicting global atmospheric ice nuclei distributions and their impacts on climate, Proc. Natl. Acad. Sci. U. S. A., 107(25), 11217-11222, 2010.

Doutriaux-Boucher, M., and Quaas, J.: Evaluation of cloud thermodynamic phase parameterizations in the LMDZ GCM by using POLDER satellite data, Geophys. Res. Lett., 31, L06126, doi:10.1029/2003GL019095, 2004.

Fu, Q.: A new parameterization of an asymmetry factor of cirrus clouds for climate models.J. Atmos. Sci., 64, 4144-4154, 2007.

Fu, Q., Sun, W.B., and Yang, P.: On modeling of scattering and absorption by nonspherical cirrus ice particles in thermal infrared wavelengths, J. Atmos. Sci., 56, 2937-2947, 1999.

Gettelman, A., Liu, X., Barahona, D., Lohmann, U., and Chen C.: Climate impacts of ice nucleation, J. Geophys. Res., 117, D20201, doi: 10.1029/2012JD017950, 2012.

Giraud, V., Thouron, O., Riedi, J., and Goloub, P.: Analysis of direct comparison of cloud top temperature and infrared split window signature against independent retrievals of cloud thermodynamic phase, Geophys. Res. Lett., 28, 983–986, 2001.

Hansen, J., Ruedy, R., Sato, M., and Lo, K.: Global surface temperature change, Rev. Geophys., 48, RG4004, doi:10.1029/2010RG000345, 2010.

Hogan, R.J., Illingworth, A.J., O'Connor, E.J., and Poiares Baptista, J.P.V.: Characteristics of mixed-phase clouds. II: A climatology from ground-based lidar, Quart. J. Roy. Meteor. Soc., 129, 2117–2134, 2003.

Hu, Y., Vaughan, M., Liu, Z., Lin, B., Yang, P., Flittner, D., Hunt, W., Kuehn, R., Huang, J., Wu, D., Rodier, S., Powell, K., Trepte, C., and Winker, D.: The depolarization-attenuated backscatter relation: CALIPSO lidar measurements vs. theory, Opt. Exp., 15, 5327–5332, 2007.

Hu, Y., Winker, D., Vaughan, M., Lin, B., Omar, A., Trepte, C., Flittner, D., Yang, P., Nasiri, S., Baum, B. A., Sun, W., Liu, Z., Wang, Z., Young, S., Stamnes, K., Huang, J., Kuehn, R., and Holz, R. E.: CALIPSO/ CALIOP cloud phase discrimination algorithm, J. Atmos. Ocean. Technol., 26, 2206–2309. DOI:10.1175/2009JTECHA1280.1, 2009.

Hu, Y., Rodier, S., Xu, K.M., Sun,W., Huang, J., Lin, B., Zhai, P., and Josset, D.: Occurrence, liquid water content, and fraction of supercooled water clouds from combined CALIOP/IIR/MODIS measurements, J. Geophys. Res., 115, D00H34, doi:10.1029/2009JD012384, 2010.

Huang, J. P., Minnis, P., and Lin, B.: Advanced retrievals of multilayered cloud properties using multispectral measurements, J. Geophys. Res., 110, D15S18, doi:10.1029/2004JD005101, 2005.

Huang, J. P., Minnis, P., and Lin, B.: Determination of ice water path in ice-over-water cloud systems using combined MODIS and AMSR-E measurements, Geophys. Res. Lett., 33, L21801, doi:10.1029/ 2006GL027038, 2006a.

Huang, J.P., Lin, B., Minnis, P., Wang, T., Wang, X., Hu, Y., Yi, Y., and Ayers, J.R.: Satellite-based assessment of possible dust aerosols semi-direct effect on cloud water path over East Asia, Geophys. Res. Lett., 33, L19802, doi: 10.1029/2006GL026561, 2006b.

Huang, J.P., Minnis, P., Lin, B., Wang, T., Yi, Y., Hu, Y., Sun-Mack, S., and Ayers, K.: Possible influences of Asian dust aerosols on cloud properties and radiative forcing observed from MODIS and CERES, Geophys. Res. Lett., 33, L06824, doi: 10.1029/2005GL024724, 2006c.

Huang, J., Wang, T., Wang, W., Li, Z., and Yan, H.: Climate effects of dust aerosols over East Asian arid and semiarid regions, J. Geophys. Res., 119, 11398–11416, doi:10.1002/2014JD021796, 2014.

Huang, Z., Huang, J., Bi, J., Wang, G., Wang, W., Fu, Q., Li, Z., Tsay, S.-C., and Shi, J.: Dust aerosol vertical structure measurements using three MPL lidars during

2008 China-U.S. joint dust field experiment, J. Geophys. Res., 115 D00K15, doi:10.1029/2009JD013273, 2010.

Intrieri, J.M., Shupe, M.D., Uttal, T., and McCarty, B.J.: An annual cycle of Arctic cloud characteristics observed by radar and lidar at SHEBA, J. Geophys. Res., 107, 8030, doi:10.1029/2000JC000423, 2002.

Kawamoto, K., Suzuki, K.: Microphysical transition in water clouds Over the Amazon and China derived from space-borne radar and Radiometer data, J. Geophys. Res., 117, D05212. http://dx.doi.org/10.1029/2011JD016412, 2012.

Kawamoto, K., Suzuki, K.: Comparison of water cloud microphysics over mid-latitude land and ocean using CloudSat and MODIS observations, J. Quant. Spectrosc. Radiat. Transf., 122, 13–24, 2013.

Klein, S. A. and Hartmann, D. L.: The seasonal cycle of low stratiform clouds, J. Clim., 6, 1588–1606, 1993.

Klein, S.A., McCoy, R. B., Morrison, H., et al.: Intercomparison of model simulations of mixed‐phase clouds observed during the ARM Mixed‐Phase Arctic Cloud Experiment, Part I: Single‐layer cloud, Quart. J. Roy. Meteor. Soc., 135, 979-1002, 2009.

Klein, S. A., Zhang, Y., Zelinka, M. D., Pincus, R., Boyle, J., and Gleckler, P. J.: Are climate model simulations of clouds improving? An evaluation using the ISCCP simulator, J. Geophys. Res., 118, 1329–1342, doi:10.1002/jgrd.50141, 2013.

Li, J., Yi, Y., Minnis, P., Huang, J., Yan, H., Ma, Y., Wang, W., Ayers, J. K.: Radiative effect differences between multi-layered and single-layer clouds derived from CERES, CALIPSO, and CloudSat data, J. Quant. Spectrosc. Radiat. Transf., 112, doi:10.1016/j.jqsrt.2010.10.006, 2010.

Li, J., Hu, Y., Huang, J., Stamnes, K., Yi, Y., and Stamnes, S.: A new method for retrieval of the extinction coefficient of water clouds by using the tail of the CALIOP signal, Atmos. Chem. Phys., 11, 1-15, 2011.

Li, J., Yi, Y. H., Stamnes, K., Ding, X. D., Wang, T. H., Jin, H. C., and Wang, S. S.: A new approach to retrieve cloud base height of marine boundary layer clouds, Geophys. Res. Lett., 40, 4448–4453, doi:10.1002/grl.50836, 2013.

Li, J., Huang, J., Stamnes, K., Wang, T., Lv, Q., and Jin, H.: A global survey of cloud overlap based on CALIPSO and CloudSat measurements, Atmos. Chem. Phys., 15, 519-536, doi:10.5194/acp-15-519-2015, 2015.

Li, Z.X., and Treut, H. Le.: Cloud-radiation feedbacks in a general circulation model and their dependence on cloud modelling assumptions, Clim. Dynam., 7, 133–139, 1992.

Liu, Y., Huang, J., Shi, G., Takamura, T., Khatri, P., Bi, J., Shi, J.,Wang, T., Wang, X., and Zhang, B.: Aerosol optical properties and radiative effect determined from sky-radiometer over Loess Plateau of Northwest China, Atmos. Chem. Phys., 11, 11455–11463, doi:10.5194/acp-11-11455-2011, 2011.

Liu, Z., Vaughan, M., Winker, D., Kittaka, C., Getzewich, B., Kuehn, R., Omar, A., Powell, K., Trepte, C., and Hostetler, C.:The CALIPSO lidar cloud and aerosol discrimination: Version 2 algorithm and initial assessment of performance, J. Atmos. Oceanic Technol., 26(7), 1198–1213, doi:10.1175/2009JTECHA1229.1, 2009.

Lohmann, U., and Feichter, J.: Global indirect aerosol effects: A review, Atmos. Chem. Phys., 5, 715–737, 2005.

Lv, Q., Li, J., Wang, T., and Huang, J.: Cloud radiative forcing induced by layered clouds and associated impact on the atmospheric heating rate, J. Meteor. Res., 29(5), 779-792, doi: 10.1007/s13351-015-5078-7, 2015.

Mielonen, T., Arola, A., Komppula, M., Kukkonen, J., Koskinen, J., Leeuw, G. de., and Lehtinen, K. E. J.: Comparison of CALIOP level 2 aerosol subtypes to aerosol types derived from AERONET inversion data, Geophys. Res. Lett., 36, L18804, doi:10.1029/2009GL039609, 2009.

Morrison, H., Shupe, M. D., and Curry, J. A.: Modeling clouds observed at SHEBA using a bulk microphysics parameterization implemented into a single-column model, J. Geophys. Res., 108, 4255, doi:10.1029/2002JD002229, 2003.

Morrison, A. E, Siems, S.T, and Manton, M. J.: A three-year climatology of cloud-top phase over the Southern Ocean and North Pacific, J. Clim., 24(9), 2405-2418, 2011.

Morrison, H., McCoy, R.B., Klein, S.A., et al.: Intercomparison of model simulations of mixed-phase clouds observed during the ARM Mixed-Phase Arctic Cloud Experiment, Part II: Multi-layered cloud, Quart, J. Roy. Meteor. Soc., 135, 1003-1019, 2009.

Naud, C.M., Del Genio, A.D., and Bauer, M.: Observational constraints on the cloud thermodynamic phase in midlatitude storms, J. Clim., 19(20), 5273-5288, 2006.

Niedermeier, D., et al.: Experimental study of the role of physicochemical surface processing on the IN ability of mineral dust particles, Atmos. Chem. Phys., 11(21), 11,131–11,144, doi:10.5194/acp-11-11131-2011, 2011.

Omar, A. H., et al.: The CALIPSO automated aerosol classification and lidar ratio selection algorithm, J. Atmos. Oceanic Technol., 26(10), 1994–2014, doi:10.1175/2009JTECHA1231.1, 2009.

Partain, P.: Cloudsat ECMWF-AUX auxiliary data process description and interface control document, Coop. Inst. for Res. in the Atmos., Colo. State Univ., Fort Collins, 2004.

Pruppacher, H. R., and Klett, J. D.: Microphysics of Clouds and Precipitation. 1st ed. Kluwer Academic, 714 pp, 1978.

Qian, W.H., Quan, L.S., and Shi, S.Y.: Variations of the dust storm in China and its climatic control, J. Clim., 15, 1216–1229, 2002.

Richardson, M. S., et al.: Measurements of heterogeneous ice nuclei in the western United States in springtime and their relation to aerosol characteristics, J. Geophys. Res., 112, D02209, doi:10.1029/2006JD007500, 2007.

Roger, R. R., and Yau, M. K.: Short Course in Cloud Physics, 3rd ed., 293 pp., Pergamon, New York, 1989.

Sassen, K., and Khvorostyanov, V.I.: Microphysical and radiative properties of mixed phase altocumulus: a model evaluation of glaciation effects. Atmos. Res., 84, 390–398, 2007.

Sassen, K. and Wang, Z.: Classifying clouds around the globe with the CloudSat radar: 1-year of results, Geophys. Res. Lett., 35, L04805, doi:10.1029/2007GL032591, 2008.

Shupe, M.D., Matrosov, S.Y., and Uttal, T.: Arctic mixed-phase cloud properties derived from surface-based sensors at SHEBA, J. Atmos. Sci., 63(2), 697-711, 2006.

Smith, R. N. B.: A scheme for predicting layer clouds and their water content in a general circulation model, Quart. J. Roy. Meteor. Soc., 116, 435–460, 1990.

Song, X., Zhang, G. J., and Li, J. L. F.: Evaluation of microphysics parameterization for convective clouds in the NCAR Community Atmosphere Model CAM5, J. Clim., 25, 8568–8590, 2012.

Stephens, G. L.: Cloud feedbacks in the climate system: a critical review, J. Clim., 18, 237–273, 2005.

Stephens, G.L., Vane, D.G., Boain, R.J., Mace, G.G., Sassen, K., Wang, Z., Illingworth, A.J., O'Connor, E.J., Rossow, W.B., Durden, S.L., Miller, S.D., Austin, R.T., Benedetti, A., Mitrescu, C., and CloudSat Science Team.: The CloudSat mission and the A-Train, A new dimension of space-based observations of clouds and precipitation, B. Am. Meteorol. Soc., 83, 1771–1790, 2002.

Storelvmo, T., Kristjánsson, J.E., and Lohmann, U.: Aerosol influence on mixed-phase clouds in CAM-Oslo, J. Atmos. Sci., 65, 3214–3230, 2008.

Su, J., Huang, J., Fu, Q., Minnis, P., Ge, J., and Bi, J.: Estimation of Asian dust aerosol effect on cloud radiation forcing using Fu-Liou radiative model and CERES measurements, Atmos. Chem. Phys., 8, 2763-2771, 2008.

Sun, W.B., Loeb, N., Videen, G., Fu, Q.: Examination of surface roughness on light scattering by long ice columns by use of a two-dimensional finite-difference time-domian algorithm, Appl. Opt., 43, 1957 – 1964, 2004.

Sun, W., Baize, R. R., Videen, G., Hu, Y., and Fu, Q.: A method to retrieve super-thin cloud optical depth over ocean background with polarized sunlight, Atmos. Chem. Phys., 15, 11909-11918, doi:10.5194/ acp-15-11909-2015, 2015.

Tan, I., Storelvmo, T., and Choi, Y.S.: Spaceborne lidar observations of the ice-nucleating potential of dust, polluted dust and smoke aerosols in mixed-phase clouds, J. Geophys. Res. Atmos., 119, 6653–6665, doi:10.1002/2013JD021333, 2014.

Tao, W. K.: Goddard cumulus ensemble (GCE) model: Application for understanding precipitation processes, Meteorol. Monogr., 29, 107–138, 2003.

Tsushima, Y., Emori, S., Ogura, T., Kimoto, M., Webb, M. J., Williams, K. D., Ringer, M. A., Soden, B. J., Li, B., and Andronova, N.: Importance of the mixed phase cloud distribution in the control climate for assessing the response of clouds to carbon dioxide increase: a multi‐model study, Clim. Dyn., 27, 113–126, 2006.

Wang, Z. and Sassen, K.: Cloud type and macrophysical property retrieval using multiple remote sensors, J. Appl. Meteor., 40, 1665–1682, 2001.

Wang, W., Huang, J., Minnis, P., Hu, Y., Li, J., Huang, Z., Ayers,J. K., and Wang, T.: Dusty cloud properties and radiative forcing over dust source and downwind regions derived from A-Train data during the Pacific Dust Experiment, J. Geophys. Res., 115, D00H35, doi:10.1029/2010JD014109, 2010.

Weidle, F., and Wernli, H.: Comparison of ERA40 cloud top phase with POLDER-1 observations, J. Geophys. Res., 113, D05209, doi:10.1029/2007JD009234, 2008.

Williams, K. D., Ringer, M. A., and Senior, C. A.: Evaluating the cloud response to climate change and current climate variability, Clim. Dynam., 20, 705–721, doi:10.1007/s00382-002-0303-3, 2003.

Winker D. M., Hunt, W. H., and Mcgill, M. J.: Initial performance assessment of CALIOP, Geophys. Res. Lett., 34, L19803, doi:10.1029/ 2007GL030135, 2007.

Yin, J.: A consistent poleward shift of the storm tracks in simulations of 21st century climate, Geophys. Res. Lett., 32, L18701, doi:10.1029/2005GL023684, 2005.

Yuan, T. and Oreopoulos, L.: On the global character of overlap between low and high clouds, Geophys. Res. Lett., 40, 5320–5326, doi:10.1002/grl.50871, 2013.

Zhang, D., Wang, Z., and Liu D.: A global view of midlevel liquid-layer topped stratiform cloud distribution and phase partition from CALIPSO and CloudSat measurements, J. Geophys. Res., 115, D00H13, doi: 10.1029/2009JD012143, 2010.

Zhang, D., Liu, D., Luo, T., Wang, Z., and Yin, Y.: Aerosol impacts on cloud thermodynamic phase change over East Asia observed with CALIPSO and CloudSat measurements, J. Geophys. Res. Atmos., 120, 1490–1501, doi:10.1002/2014JD022630, 2015.

Zhang, M. H., Lin, W. Y., Klein, S. A., Bacmeister, J. T., Bony, S., Cederwall, R. T., Del Genio, A.D., Hack, J. J., Loeb, N. G., Lohmann, U., Minnis, P., Musat, I., Pincus, R., Stier, P., Suarez,M. J., Webb, M. J., Wu, J. B., Xie, S. C., Yao, M. S., and Zhang, J. H.: Comparing clouds and 15 their seasonal variations in 10 atmospheric general circulation models with satellite measurements, J. Geophys. Res., 110, D15S02, doi:10.1029/2004JD005021, 2005.

Zhu, C., Wang, B., and Qian, W.: Why do dust storms decrease in northern China concurrently with the recent global warming?, Geophys. Res. Lett., 35, L18702, doi:10.1029/2008GL034886, 2008.

Atmos. Chem. Phys. Discuss., doi:10.5194/acp-2016-147, 2016
Manuscript under review for journal Atmos. Chem. Phys.
Published: 25 February 2016

Atmospheric Chemistry and Physics
Open Access
Discussions

Table1. Cloud phase partitioning schemes used in different climate models (cited from the table 1 of Choi et al. (2014).

GCM	reference	Scheme[a]	$T_{ice,}$ °C	T_w, °C	n
ERA40	(Weidle and Wernli (2008))	1	-23	0	2
CAM3	(Collins et al. (2004))	1	-40	-10	1
CAM5	(Song et al. (2012))	1	-35	-5	1
GISS, Land	(Del Genio et al. (1996))	2	-40	-10	2
GISS, Ocean	(Del Genio et al. (1996))	2	-40	-4	2
LMDZ(standard version)	(Doutriaux-Boucher and Quaas (2004))	1	-15	0	6
LMDZ(modified version	(Doutriaux-Boucher and Quaas (2004))	1	-32	0	1.7

[a] Scheme 1: water cloud fraction $f=\left(\frac{T-T_{ice}}{T_w-T}\right)^n$, here $T_{ice} \le T \le T_w$

[a] Scheme 2: water cloud fraction $f=\exp[-(\frac{T_w-T}{15})^n]$, here $T_{ice} \le T \le T_w$

Atmos. Chem. Phys. Discuss., doi:10.5194/acp-2016-147, 2016
Manuscript under review for journal Atmos. Chem. Phys.
Published: 25 February 2016

Figure Captions

Fig.1. The geographic and seasonal variations of T_w value over 2º×6º grid boxes based on the 2B-CLDCLASS-Lidar product.

Fig.2. The geographic and seasonal variations of T_{ice} value over 2º×6º grid boxes based on the 2B-CLDCLASS-Lidar product.

Fig. 3. Parameter n vs the mean supercooled water cloud fraction between -40ºC to 0ºC. The color presents the numbers of grid.

Fig.4. The geographic and seasonal variations of parameter n over 2º×6º grid boxes based on the 2B-CLDCLASS-Lidar product.

Fig.5. The geographic and seasonal variations of the grid mean value of absolute difference (annual mean) between calculated and observed SCFs for different schemes, respectively. (a) for the scheme 1 used the dynamical thresholds of T_{ice}, T_w and n; (b) for the scheme 2 used the dynamical thresholds of T_{ice}, T_w and n; (c) for the CAM3; and (d) for the CAM5.

Fig.6. The geographic and seasonal variations of the grid mean value of relative difference (annual mean) between calculated and observed SCFs for different schemes, respectively. (a) for the scheme 1 used the dynamical thresholds of T_{ice}, T_w and n; (b) for the scheme 2 used the dynamical thresholds of T_{ice}, T_w and n; (c) for the CAM3; and (d) for the CAM5.

Fig.7. (a) The observed vertical distribution of zonal mean SCF with temperature; and the difference of vertical distribution between calculated and observed SCFs, (b) for the scheme 1 used the dynamical thresholds of T_{ice}, T_w and n; (c) for the CAM3; and (d) for the CAM5.

Fig.8. The geographic and seasonal variations of supercooled water cloud fraction at -20ºC over 2º×6º grid boxes.

Fig.9. The geographic and seasonal variations of relative aerosol occurrence frequency (RAOF) at -20ºC over 2º×6º grid boxes based on the CALIPSO level 2 5 km aerosol level product.

Fig.10. The seasonal and zonal variations of SCF and RAOF at -20ºC, LTSS and 500hPa vertical velocity.

Fig.11. The geographic and seasonal variations of the 50% supercooled water cloud fraction-Top temperature (T_{50}) over 2º×6º grid boxes.

Atmos. Chem. Phys. Discuss., doi:10.5194/acp-2016-147, 2016
Manuscript under review for journal Atmos. Chem. Phys.
Published: 25 February 2016

Fig.12. The dependences of T_{50}, n and SCF at -20ºC on the RAOF and 500hPa vertical velocity. The error bars correspond to the ±5 standard error.

Fig.13. The dependences of T_{50}, n and SCF at -20ºC on the RAOF and surface temperature. The error bars correspond to the ±5 standard error.

Fig.14. The dependences of T_{50}, n and SCF at -20ºC on the RAOF and LTSS. The error bars correspond to the ±5 standard error.

Atmos. Chem. Phys. Discuss., doi:10.5194/acp-2016-147, 2016
Manuscript under review for journal Atmos. Chem. Phys.
Published: 25 February 2016

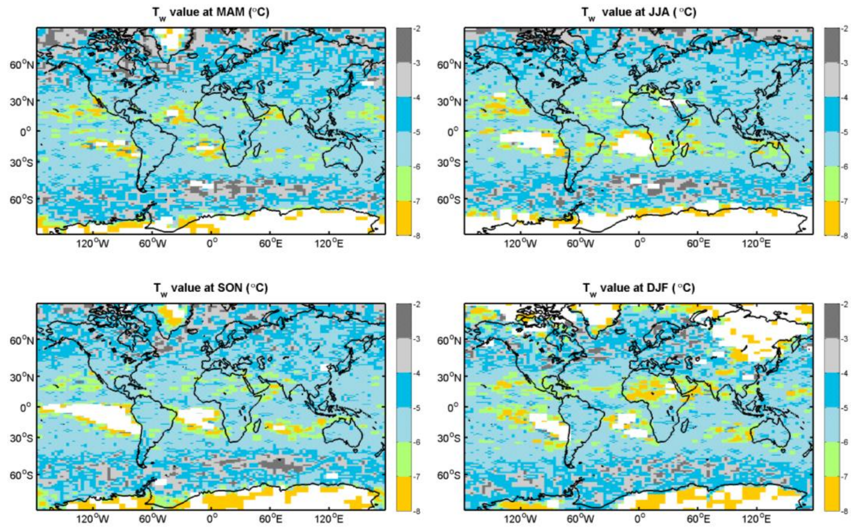

Fig.1. The geographic and seasonal variations of T_w value over 2°×6° grid boxes based on the 2B-CLDCLASS-Lidar product.

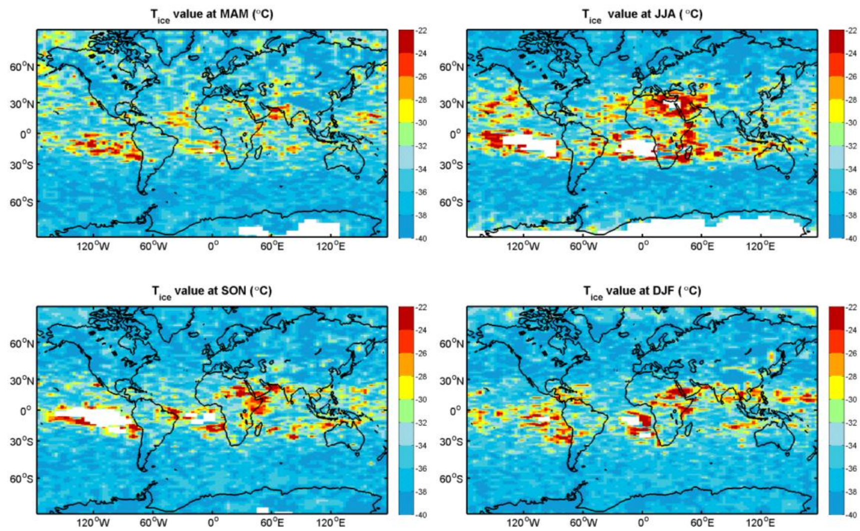

Fig.2. The geographic and seasonal variations of T_{ice} value over 2°×6° grid boxes based on the 2B-CLDCLASS-Lidar product.

Atmos. Chem. Phys. Discuss., doi:10.5194/acp-2016-147, 2016
Manuscript under review for journal Atmos. Chem. Phys.
Published: 25 February 2016

Atmospheric Chemistry and Physics
Open Access
Discussions

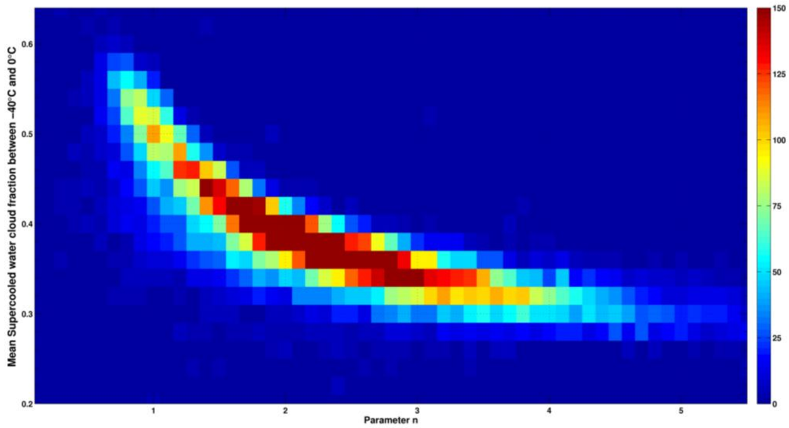

Fig. 3. Parameter *n* vs the mean supercooled water cloud fraction between -40 ℃ to 0 ℃. The color presents the numbers of grid.

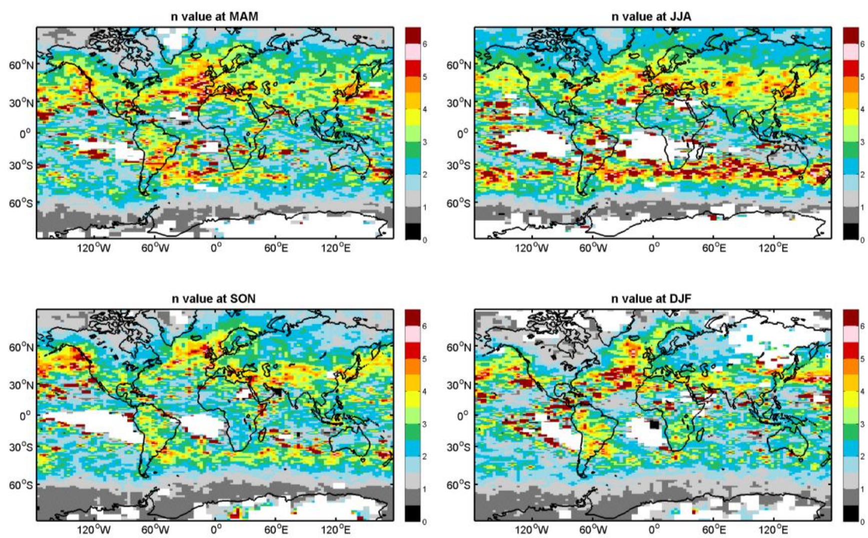

Fig.4. The geographic and seasonal variations of parameter *n* over 2°×6° grid boxes based on the 2B-CLDCLASS-Lidar product.

Atmos. Chem. Phys. Discuss., doi:10.5194/acp-2016-147, 2016
Manuscript under review for journal Atmos. Chem. Phys.
Published: 25 February 2016

Atmospheric Chemistry and Physics
Discussions

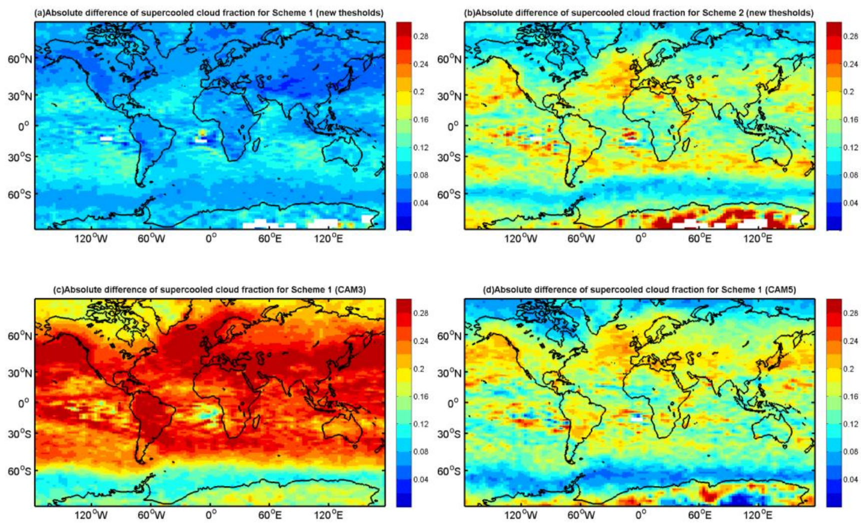

Fig.5. The geographic and seasonal variations of the grid mean value of absolute difference (annual mean) between calculated and observed SCFs for different schemes, respectively. (a) for the scheme 1 used the dynamical thresholds of T_{ice}, T_w and n; (b) for the scheme 2 used the dynamical thresholds of T_{ice}, T_w and n; (c) for the CAM3; and (d) for the CAM5.

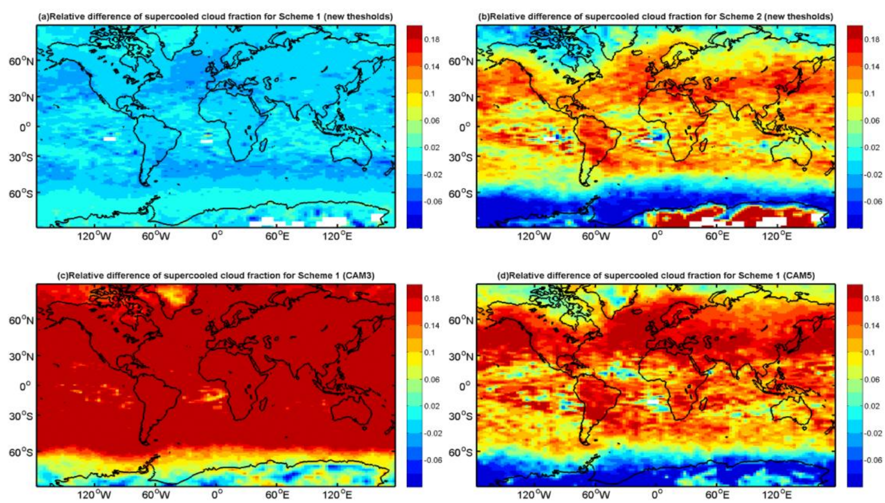

Fig.6. The geographic and seasonal variations of the grid mean value of relative difference (annual mean) between calculated and observed SCFs for different schemes, respectively. (a) for the scheme 1 used the dynamical thresholds of T_{ice}, T_w and n; (b) for the scheme 2 used the dynamical thresholds of T_{ice}, T_w and n; (c) for the CAM3; and (d) for the CAM5.

Atmos. Chem. Phys. Discuss., doi:10.5194/acp-2016-147, 2016
Manuscript under review for journal Atmos. Chem. Phys.
Published: 25 February 2016

Atmospheric Chemistry and Physics
Open Access
Discussions

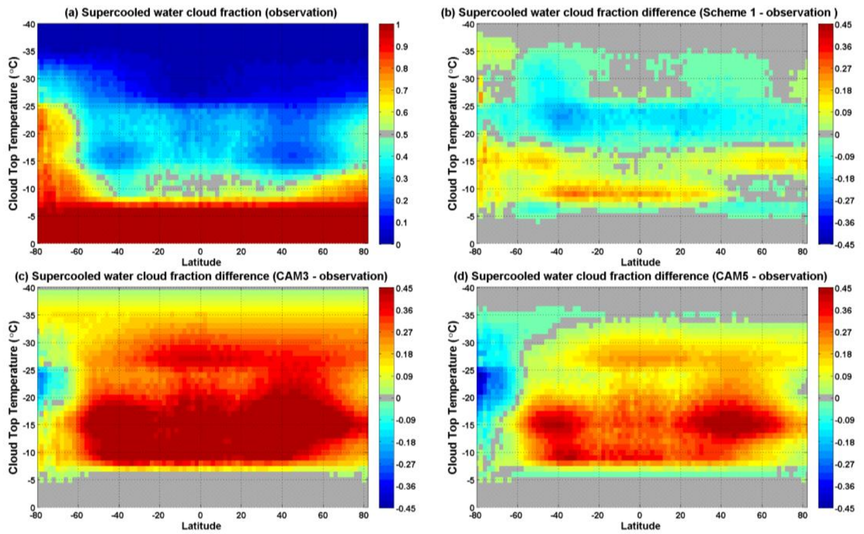

Fig.7. (a) The observed vertical distribution of zonal mean SCF with temperature; and the difference of vertical distribution between calculated and observed SCFs, (b) for the scheme 1 used the dynamical thresholds of T_{ice}, T_w and n; (c) for the CAM3; and (d) for the CAM5.

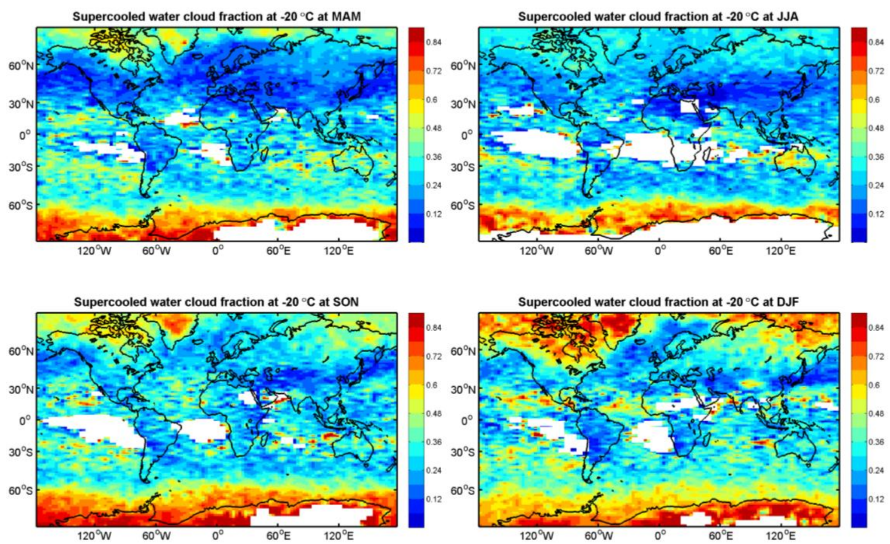

Fig.8. The geographic and seasonal variations of supercooled water cloud fraction at -20 ℃ over 2°×6° grid boxes.

Atmos. Chem. Phys. Discuss., doi:10.5194/acp-2016-147, 2016
Manuscript under review for journal Atmos. Chem. Phys.
Published: 25 February 2016

Atmospheric Chemistry and Physics
Open Access
Discussions

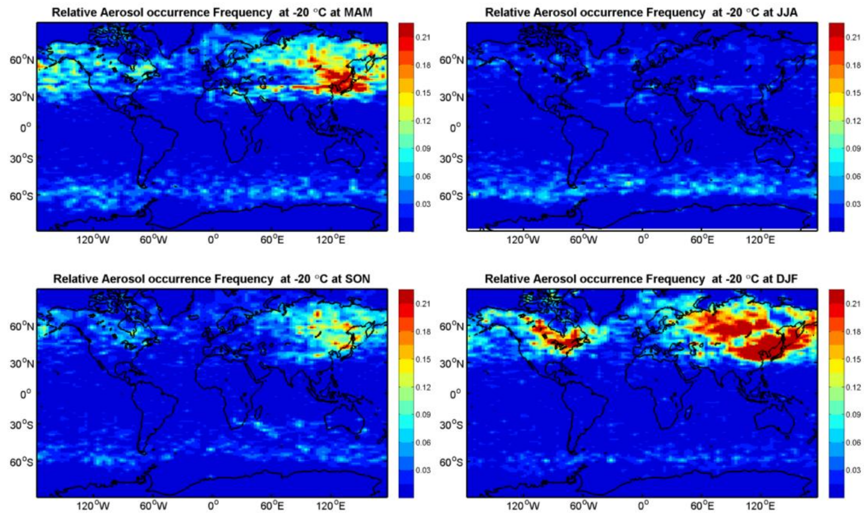

Fig.9. The geographic and seasonal variations of relative aerosol occurrence frequency (RAOF) at -20 ℃ over 2°×6° grid boxes based on the CALIPSO level 2 5 km aerosol level product.

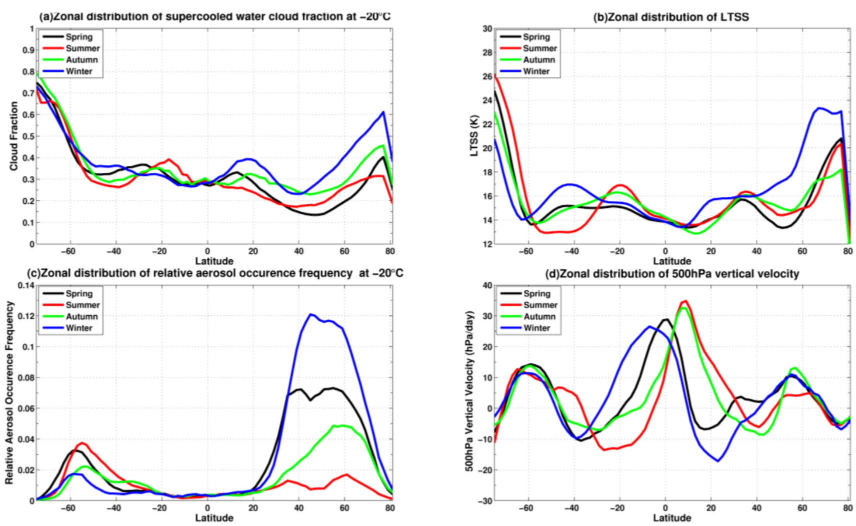

Fig.10. The seasonal and zonal variations of SCF and RAOF at -20 ℃, LTSS and 500hPa vertical velocity.

Atmos. Chem. Phys. Discuss., doi:10.5194/acp-2016-147, 2016
Manuscript under review for journal Atmos. Chem. Phys.
Published: 25 February 2016

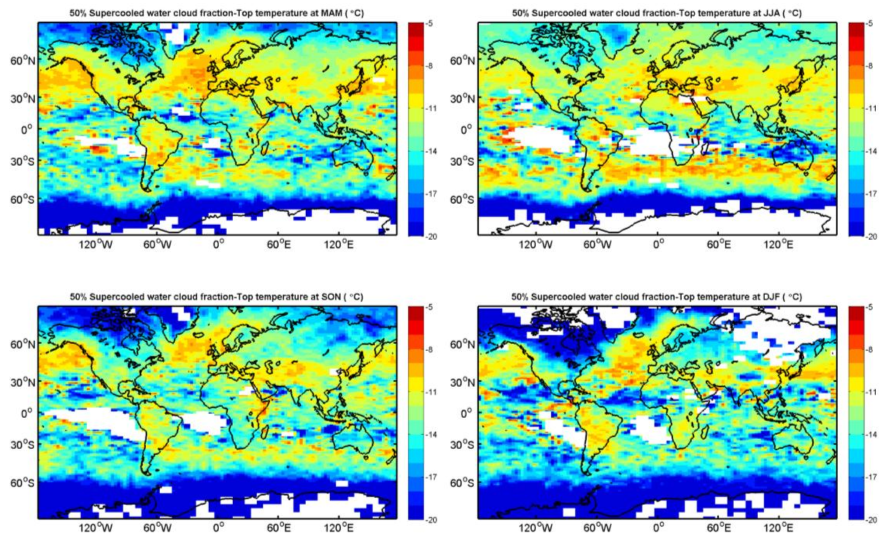

Fig.11. The geographic and seasonal variations of the 50% supercooled water cloud fraction-Top temperature (T_{50}) over 2°×6° grid boxes .

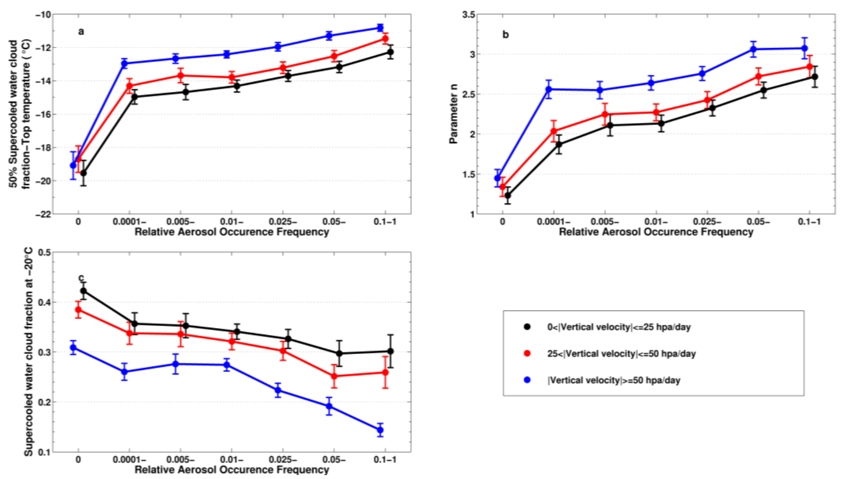

Fig.12. The dependences of T_{50}, n and SCF at -20℃ on the RAOF and 500hPa vertical velocity. The error bars correspond to the ±5 standard error.

Atmos. Chem. Phys. Discuss., doi:10.5194/acp-2016-147, 2016
Manuscript under review for journal Atmos. Chem. Phys.
Published: 25 February 2016

Atmospheric Chemistry and Physics
Open Access
Discussions

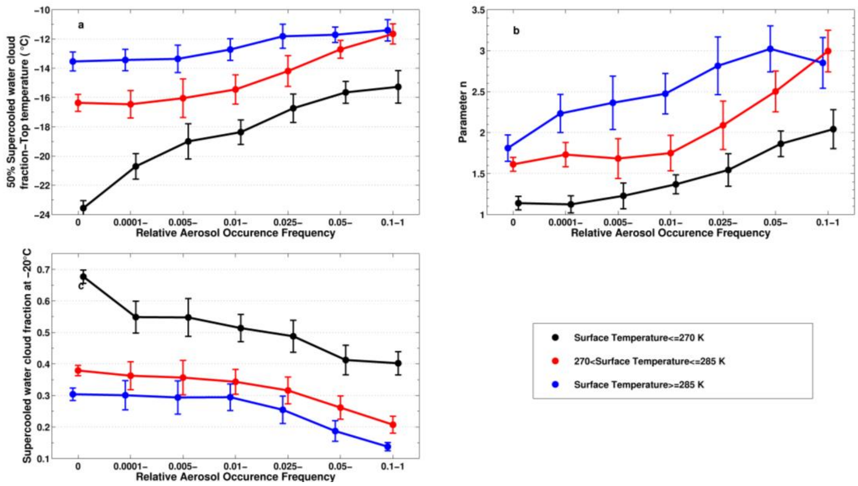

Fig.13. The dependences of T_{50}, n and SCF at -20 ℃ on the RAOF and surface temperature. The error bars correspond to the ±5 standard error.

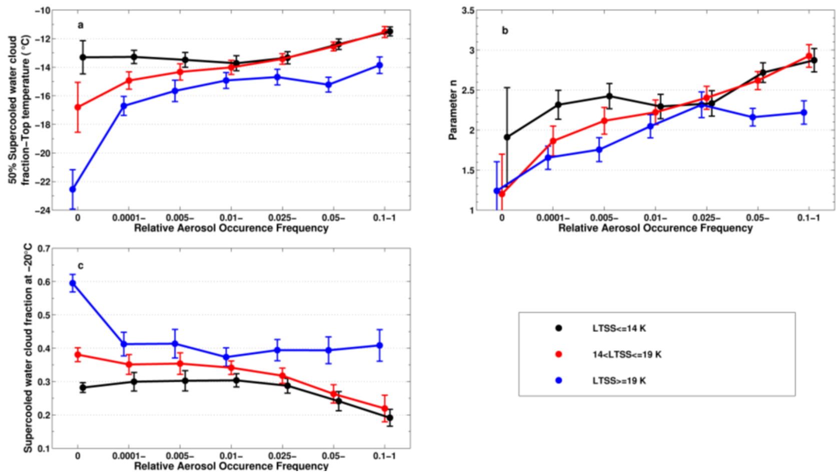

Fig.14. The dependences of T_{50}, n and SCF at -20 ℃ on the RAOF and LTSS. The error bars correspond to the ±5 standard error.